



Influence of welding stresses on relief cracking during heat treatment of a creep-resistant 13CrMoV steel Part II: mechanisms of stress relief cracking during post weld heat treatment

A. Kromm¹ · T. Lausch¹ · D. Schroepfer¹ · M. Rhode^{1,2} · T. Kannengiesser^{1,2}

Received: 27 December 2019 / Accepted: 2 March 2020 / Published online: 12 March 2020
© The Author(s) 2020, corrected publication 2021

Abstract

Welding of 13CrMoV9-10 vanadium steel requires care due to an increased susceptibility to stress relief cracking during post weld heat treatment. Previous research into the crack formation in creep-resistant steels has focused on thermal and metallurgical factors; however, little knowledge has been gathered regarding the crack formation during post weld heat treatment considering real-life restraint conditions. This work is subdivided in two parts. Part I showed that an increasing heat input during submerged arc welding under restraint led to an increasing stress level in the joint prior to the post weld heat treatment. The magnitude of stress relief cracking observed in the heat-affected zone after the post weld heat treatment is affected by the heat input. In Part II of this work, the cracks and the associated microstructure which occurred under restraint were studied. The application of a special acoustic emission analysis indicated that the cracks formed in a temperature range between 300 and 500 °C during the post weld heat treatment. The toughness in the heat-affected zone of the restrained welds was affected by the welding heat input. Microstructural analyses of all specimens revealed accelerated aging due to precipitation of carbides during post weld heat treatment under restraint.

Keywords Welding · Creep-resistant steel · Post weld heat treatment · Stress relief cracking

1 Introduction

The creep resistant steel 13CrMoV9-10, a modified conventional low-alloyed 2.25Cr-1Mo steel with 0.25% vanadium is highly sensitive to stress relief cracking (SRC) during post weld heat treatment (PWHT). PWHT is applied after welding and necessary to adjust the mechanical properties in the weld metal and the heat-affected zone (HAZ) as well as to reduce welding-related structural and residual stresses. Although the basic mechanisms of SRC are generally known and widely documented in the literature, the influence and control factors

as well as the detailed mechanisms of crack formation continue to be controversially discussed. In general, SRC occurs when stresses during heat treatment exceed the local deformation capacity of the material. In principle, the following mechanisms are necessary:

- Almost complete dissolution of carbides and carbonitrides in the weld boundary (coarse grained HAZ) area during welding.
- Partial solution (supersaturation) of the carbide-forming elements due to rapid cooling after welding
- Separation of the dissolved elements and formation of carbides in the matrix during further PWHT

There is agreement on the origin of the crack that precipitation processes lead to differences in strength between the grain boundary regions and the interior of the grain. Because of the lower strength, the relaxation processes largely take place via sliding processes in the grain boundary regions. The crack propagation occurs along the prior austenite grain boundaries (PAGB) and leads to the typical, predominantly intergranular separation. However, different positions can be

Recommended for publication by Commission II - Arc Welding and Filler Metals

✉ A. Kromm
arne.kromm@bam.de

¹ Bundesanstalt für Materialforschung und -prüfung (BAM), Berlin, Germany

² Institute for Materials Science and Joining Technology, Otto-von-Guericke-University, Magdeburg, Germany

found regarding the precipitation mechanisms effective in SRC and the resulting solidification or softening of the grain boundary regions or the interior of the grain:

- Precipitation of mostly incoherent carbides such as Fe_3C , M_{23}C_6 , or M_6C on the PAGB leads to weakening of the grain boundaries and thus to material separation during stress relief heat treatment [1–5].
- (Film-like) enrichment of certain alloying elements and impurity element segregation (P, S, Sb, Sn, As) to the PAGB lead to grain boundary separation during stress-relief heat treatment due to flow processes [4, 6–12].
- Fine-dispersed (usually coherent) precipitates in the grain interior (e.g., V_4V_3 , Mo_2C) cause an increase in strength of the (ferrite) grains compared with the PAGB, so that flow processes can only take place via sliding along the weaker grain boundary regions, which can lead to the formation of pores and ultimately to material separation [1, 4, 7, 13–17].

In order to evaluate the cracking susceptibility of high-temperature low-alloy steels, several researchers have developed formulas based on the chemical compositions of filler and base materials. By extensive empirical investigations, they tried to quantify the effects of certain alloying elements by evaluation factors. The calculation approaches commonly used today for estimating SRC sensitivity are the Bruscato factor [9] and the Watanabe factor [18]. A more recent approach, still under discussion, is the K -factor according to Chauvy and Pillot [6, 19, 20].

Bruscato [9] presented an approach for the assessment of the cracking sensitivity, which for the first time considered the harmful effect of tramp elements in steel. The so-called X factor (temper embrittlement factor) is based on investigations on 2.25Cr-1Mo steels and serves to evaluate the tendency to temper embrittlement based on P, Sb, Sn, and As cf., Eq. 1. Bruscato also pointed out the importance of the Mn and Si content. Relationship of Bruscato [9] (contents in ppm):

$$X = (10P + 5Sb + 4Sn + As)/100 \quad (1)$$

The Bruscato factor applies to both the base metal and the weld metal. The sensitivity to cracking increases with higher values. Values < 10 ppm indicate good resistance to temper embrittlement [21].

In 1974, Watanabe et al. [18] presented the J-factor for the evaluation of the tendency to embrittlement of creep-resistant materials. The J-factor applies to the base material and is a function of the alloying elements (Mn, Si) and the tramp elements (P, Sn) cf., Eq. 2. Relationship by Watanabe et al. [18] (contents in wt.%):

$$J = (\text{Mn} + \text{Si}) \times (\text{P} + \text{Sn}) \times 10^4 \quad (2)$$

For the base metal, values of $J \leq 100$ ppm according to the current API Recommended Practice 934-A [4] are usually required in practice today.

As a result of several occurrences of failure during welding of large reactors made of Cr-Mo-V steels, Chauvy and Pillot investigated different wire/flux combinations regarding its SRC susceptibility. They presented a new criterion for evaluating the cracking sensitivity of the weld metal [6, 19, 20]. The K -factor is a function of the elements Pb, Bi, and Sb (cf., Eq. 3) and is based on investigations on 25 different wire/flux combinations already used in vessel production. Relationship of Chauvy and Pillot (contents in ppm):

$$K = \text{Pb} + \text{Bi} + 0.03\text{Sb} \quad (3)$$

Chauvy and Pillot [6, 19, 20] used the reduction of area (RoA%) in the RHC test (Reheat Cracking Test), a Gleeble tensile test at 650 °C, as an indicator of the cracking sensitivity. They deduce the following mathematical model from the results of the tensile tests and the calculated K -factors (see Eq. 4):

$$\text{RoA}\% = 13.4 + 27.3 \times e^{(-0.69 \times K)} \quad (4)$$

The reduction of area shows a visible drop from a K -factor of about 2 ppm. In the Gleeble tensile tests carried out, all weld metals in which no cracks occurred during industrial processing achieved a minimum reduction in area of 23%. Chauvy and Pillot concluded a K -factor < 1.5 ppm for a crack-resistant weld metal. The K -factor thus represents one of the most severe evaluation criteria. It considers for the first time the effects of Pb and Bi in the evaluation of the SRC sensitivity. Due to the high purity of modern steel grades, Chauvy and Pillot [6] attributed the cracking sensitivity of the steel 13CrMoV9-10 to the effect of the tramp elements Pb, Bi, and Sb. They emphasize that the determination of such low contents of impurities requires the use of high-resolution analytical techniques such as glow discharge mass spectrometry (GDMS) in order to avoid misinterpretation of materials. This conclusion was also drawn from an IIW round robin test on the measurement of trace elements in creep-resistant weld metal [22].

The criterion $K = 1.5$ ppm formulated by Chauvy and Pillot has not yet been completely confirmed by other studies. Thus Trent [23] found out that in laboratory tests with the so-called “C-ring” test crack-free weld metal was achieved even with K -factors > 1.5 ppm. The C-ring test is a severe test procedure for laboratory samples that has the advantage of applying a defined test load. At the same time, however, this has the disadvantage that the test load identified as critical cannot easily be transferred to real welds. This is because the (residual) stresses resulting from the welding process remain unknown and unconsidered.

Another common test method is the already mentioned Gleeble tensile test, which has the advantage of describing the SRC susceptibility by means of a material property. For this purpose, the reduction of area is determined as a function of temperature. Since the actual heat treatment of the specimens is generally not carried out under load, stress effects on the microstructure or the precipitation behavior are usually not considered in the Gleeble test.

Numerous other test methods have been developed over the last 60 years to investigate crack formation during stress relief heat treatment and to evaluate the cracking sensitivity of different steel grades. Already at the end of the 1970s, Dhooze et al. [12] presented 26 different test methods and evaluated their significance and reproducibility. According to this, there are basically three possible forms of testing.

First, there is the testing of a welded joint prepared on the laboratory scale in which the entire weld seam, which reflects as closely as possible the weld configuration of the real component, is subjected to a post-weld heat treatment. If cracking occurs, the PWHT is followed by metallurgical preparation of the specimens and an evaluation of the cracks. However, the shrinkage restraint in real welded joints is usually considerably higher than in small laboratory specimens and therefore a dependency between specimen size and cracking probability is not covered. Furthermore, tests on complete welds usually show a higher scatter of the results due to numerous disturbance variables, which makes it difficult to classify the cracking sensitivity accurately. Nevertheless, some test methods show good agreement with experience in practice.

Second, there are test methods in which the specimens contain just parts of the weld seam. This can be done by simply over-welding the test area or by taking samples from completely welded seams. The advantages of these test methods are, on the one hand, the rapid and cost-effective realization of the tests and, on the other hand, better reproducibility. In addition, the test load can be varied in case of externally loaded tests and therefore critical loads be determined. Prominent examples are the (modified) implant test [24] or the C-ring test [23]. The result is often a ranking of the tested materials, but transferability to practice is not always possible.

Third is the testing of samples containing a thermally simulated HAZ. This is obtained before or during the test by means of an artificial welding temperature cycle. The welding simulation enables a good reproducibility as well as the targeted adjustability of the microstructure to be tested (also multilayer welding cycles). Furthermore, it is possible to introduce notches and thus concentrate the test area on a specific microstructure. A disadvantage, however, is the neglect of welding residual stresses combined with limited transferability to real welded components.

The stress-relief heat treatment of pressure vessels made of creep-resistant steels for petrochemical reactors generally takes place after completion of all welding processing steps

by final heat treatment of the complete vessel. The processing and heat treatment of low-alloy Cr-Mo-(V)-steels is generally carried out according to the customer's specifications. Furthermore, processing recommendations for different Cr-Mo-(V) steels can be found in API Recommended Practice 934-A, DIN EN 10028-2 and AWS D10.8 [4, 25, 26]. For the V-modified 13CrMoV9-10, temperatures from 705 to 710 °C and holding times between 8 and 10 h are necessary to achieve a sufficiently high level of toughness [9, 27].

The PWHT temperature and holding time depend on the chemical composition and especially on the weld joint thickness. In cases where the mechanical stresses are already too high, it can be necessary to perform a so-called ISR (intermediate stress relief) heat treatment.

Numerous research results on precipitation behavior and carbide development in low-alloy steels have been published in the last 60 years. While there is agreement in the literature that crack initiation takes place during the heating phase of the PWHT, there are widely differing statements on the critical temperature range of crack formation, from which a very broad range between 315 and 705 °C can be derived. While the time-temperature behavior of carbide formation is documented in detail, the influence of stresses and residual stresses on carbide formation has so far received little attention. Under the assumption that stresses affect the lattice strain and thus the diffusion behavior within the matrix, it can be expected, that these also influence carbide formation analogously to temperature. For this purpose, investigations are necessary in which, in addition to temperature control, realistic stress scenarios are also implemented in laboratory tests.

2 Experimental procedure

The experiments performed in this study were carried out on the low-alloy, carbide-forming, creep-resistant pressure vessel steel 13CrMoV9-10 (1.7703) using a welding filler of the same type (ISO 24598-A – S Z CrMoV2, ISO 24598-B – SU 2C1MV). Tables 1 and 2 show the chemical composition and the mechanical properties of the base material.

The chemical analysis of the tramp elements of the weld metal and the base metal is shown in Table 3. The tramp elements were measured by mass spectrometry and spark emission spectroscopy, respectively. The Bi content was solely determined for the weld metal. With the help of the chemical composition, the factors according to Bruscati, Watanabe

Table 1 Chemical composition of 13CrMoV9-10 (spark emission spectrometric analysis) in wt.%

C	Si	Mn	Cr	Cu	Mo	Ni	Ti	V	Nb	Fe
0.12	0.08	0.51	2.29	0.11	0.98	0.12	<0.01	0.30	0.03	Balance

Table 2 Mechanical properties of 13CrMoV9-10 (hardened + tempered), manufacturer's data

Temperature in °C	Rolling direction	Yield strength $R_{p0.2}$ in MPa	Tensile strength R_m in MPa	Elongation at fracture A_5 in %	Reduction of area Z in %
RT	Longitudinal	609	714	24	80
450		491	574	20	79
RT	Transverse	621	726	22	77
450		494	576	19	77

as well as Chauvy and Pillot were calculated, which are also shown in Table 3.

Bruscatto and Watanabe factor clearly meet the common requirements, e.g., according to API [4]. The K -factor is above the limit value defined by Chauvy and Pillot for the weld metal. In Gleeble tests to determine the reduction in area as a function of the temperature of the weld metal, nevertheless, minimum values of 30% were obtained for the wire/flux combination used here [28], which is above the threshold of 23% determined by Chauvy and Pillot.

The test welds of this study were produced by varying the preheat/interpass temperature as well as the heat input per unit length during submerged arc tandem welding (SAW) using the design of experiments (DoE). The heat input per unit length was varied between 20 and 50 kJ/cm. The preheat/interpass temperature range was 180 to 260 °C. The details of welding are described in Part I of this study [29]. A special 2-MN test facility [30, 31] was used to simulate real life-like restraint conditions and allowed for observing the reaction stresses formed during welding. Two plates each with the dimensions 980 mm (l) × 250 mm (w) × 20 mm (h) were joined and subsequently heat treated. First a dehydrogenation heat treatment (DHT) was applied at 350 °C for 2 h. After cooling to ambient temperature, a post weld heat treatment (PWHT) at 705 °C was performed for 8 h. Preheating, DHT, and PWHT were realized by heating mats on the top and bottom side of the joints. The temperature was controlled by

Table 3 Tramp elements in base metal, weld metal in wt.% and associated SRC factors in ppm

	Base metal	Weld metal
P	0.005	0.0062
Sb	< 0.0005	0.00064
Sn	< 0.001	0.00017
As	0.006	0.0009
Mn	0.5	1.23
Si	0.09	0.08
Pb	0.001	< 0.0002
Bi	–	0.00001
Bruscatto (X -) factor [9]	6.25	6.678
Watanabe (J -) factor [18]	35.4	83.447
Chauvy (K -) factor [6, 19, 20]	–	2.292

a thermocouple attached to the bottom side of the specimen. Figure 1 shows exemplarily the test sequence. Table 4 gives details about the individual steps.

During preheating, welding, and dehydrogenation heat treatment (DHT), the system simulated the joining of two ring segments of a pressure vessel by restrained expansion and shrinkage of the specimen. In real component welds, the ring segments impede the expansion of the locally heated weld area. After the DHT, the specimen cools down to ambient temperature with shrinkage restraint. The stress-relief heat treatment usually takes place after welding of the entire component. The pressure vessel is heat-treated in a large furnace. Due to the almost homogeneous and slow heating, the vessel can expand freely, whereby the load resulting from the welding process remains until the necessary hot yield strength is reached. To simulate this behavior, the testing facility maintained the load level resulting from the welding process up to the prescribed annealing temperature of 705 °C and compensated for the temperature-induced expansion of the weld area. After reaching the target temperature, the system enabled the relaxation of the welded joint during cooling to room temperature.

In Part I of this study [29], it was found that the reaction stress induced by restrained welding is controlled mainly by the heat input. An increasing heat input correlates with higher reaction stresses. While all test welds under restraint showed cracks during subsequent post weld heat treatment, the amount of cracking was highest with highest heat input. The cracks were detected by magnetic particle inspection (cf., [29]).

In order to detect the temperature at which the observed cracks were formed, acoustic emission analysis was applied during the PWHT. The system consists of four sensors with a frequency range between 100 and 450 kHz. The sensor type is especially optimized for on-site tests on pressure vessels and pipelines. The analysis was performed on three of the nine test welds conducted. After hydrogen annealing and cooling of the specimens to room temperature, the sensors were fixed in a distance of 235 mm from the center of the weld using magnetic holders. To protect the sensors from overheating, water-flowing heat sinks were attached to the top and bottom of the plates between the furnace and the sensors. The threshold for signal acquisition was set to 85 dB, which is above the high background noise of the 2-MN test facility. The background

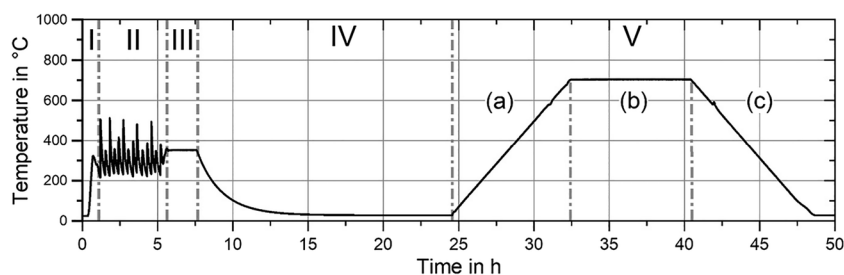


Fig. 1 Temperature control during the simulated manufacturing process in the 2-MN test facility, (I): tacking + preheating, (II): welding, (III): DHT, (IV): cooling to ambient temperature, (V): PWHT (heating (a),

holding (b), cooling (c), (preheating/interpass temperature 220 °C and heat input per unit length 35 kJ/cm)

noise was determined during the heat treatment of a dummy sample without crack formation. Unfortunately, the noise did not allow the localization of the crack formation. The recorded signal was synchronized with the simultaneously registered temperature of the specimens.

From each joint, six notched bar impact specimens were extracted to characterize the influence of the microstructure on the mechanical properties of the HAZ. The specimens were taken from locations without cracks. To characterize the occurring cracks, metallographic examinations were carried out using light microscopy (etchant: Nital) accompanied by transmission electron microscopy (TEM) and scanning electron microscopy (SEM) analyses for selected areas. The samples were taken from similar positions in the joints and compared to that of specimens from equivalent welds produced without restraint using the same welding and heat treatment parameters.

3 Results

During PWHT, the signals from the acoustic sensors mounted on the specimen were recorded at a sampling rate of 5 kHz. The results can be found in Fig. 2. The maximum amplitudes of the localized acoustic emission events and the furnace temperature as a function of time are shown. The diagram shows exemplarily the results from the PWHT of two test welds.

While at the beginning of the heat treatment, only isolated acoustic emission events below 85 dB are registered; from a temperature of approx. 300 °C, an abrupt increase in detected

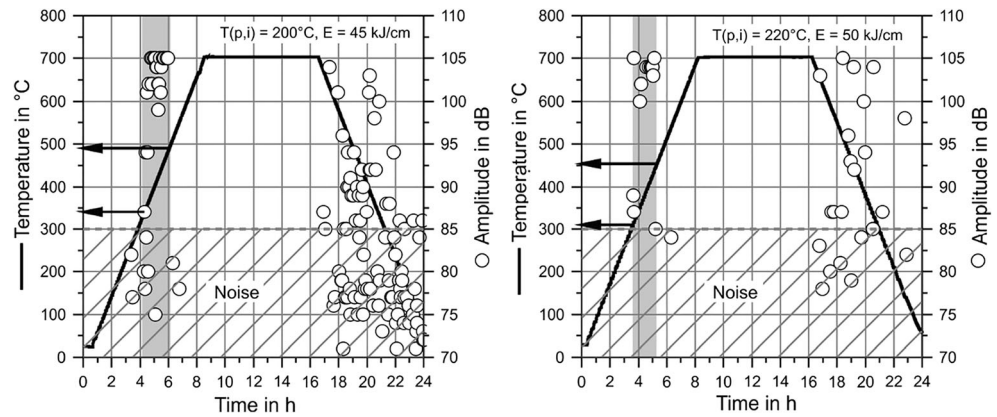
events occurs, cf., gray areas in Fig. 2. The sudden increase in acoustic emission events and the high maximum amplitudes are clear indications of initiating crack events in which the elastically stored energy is suddenly released. From a temperature of approx. 500 °C and during relaxation at 705 °C, no acoustic emission events with maximum amplitudes above 85 dB are detected, which indicates that no more cracks are initiated in the material. The continuing crack growth is accompanied by a lower energy release but cannot be distinguished from the interference signals due to the high noise signal. On the other hand, there is an increase of the detected acoustic emission events during the cooling phase. However, this is not attributable to further crack formation but are caused by the flaking of the oxide layer which formed on the sample surface during the heat treatment. The crack formation therefore took place between 300 and 500 °C with the slow heating rate (60 K/h) applied in this study. That means cracking is located in the lower temperature range between 315 and 705 °C documented in the literature [6, 32].

Figure 3 shows the notched bar impact values determined in the HAZ. The transition temperature increases with increasing welding heat input. The reason for this is the influence of the heat input on the microstructure in the HAZ, in particular the coarse-grained heat affected zone (CGHAZ) and the overlap areas of the multi-layer weld. An exception is the curve for the smallest heat input ($T_{p,i} = 220$ °C, $E = 20$ kJ/cm). Due to the formation of martensite ($t_{8/5} < 30$ s), the transition temperature also shifts to the right. In summary, it can be stated that the mechanical properties were influenced by the heat input when welding under restraint, which manifests itself with

Table 4 Welding parameters and heat treatment parameters

Step		
I	Tacking + Preheating	Tack welding and subsequent heating to the individual preheating temperature
II	Welding	Welding following the individual interpass temperature
III	DHT	350 °C for 2 h
IV	Cooling	Cooling to ambient temperature
V	PWHT (a)	Heating to 705 °C by 60 K/h
	(b)	Holding at 705 °C for 8 h
	(c)	Cooling to ambient temperature by 60 K/h

Fig. 2 Temperature and detected maximum amplitude as functions of time, during PWHT, the critical temperature range for crack initiation is highlighted in gray



increasing heat input in a shift of the transition temperature towards higher temperatures. The transition temperatures found for each heat-affected zone are higher than that for the base material. In the latter, the 54 J transition temperature ($T_{H(54 J)}$) was determined to -165°C . Even a step cooling heat treatment following [4, 25] used to simulate and accelerate embrittlement resulted in a shift of the 54 J transition temperature of less than 10°C towards higher temperatures.

The welding heat control and the associated microstructure had a significant effect on the SRC formation during PWHT under restraint. During all tests, the cracks mainly occurred at the transition of the weld metal into the HAZ (weld toe), promoted by the stress rise due to the notch effect here. This was unexpected as the factors which evaluate the impact of tramp elements (e.g., Table 3) on the embrittlement of the base material show uncritical values. The reasons for cracking during PWHT in this study are probably less related to impurities. Rather, carbide precipitation on the grain boundaries is believed to be the dominating factor.

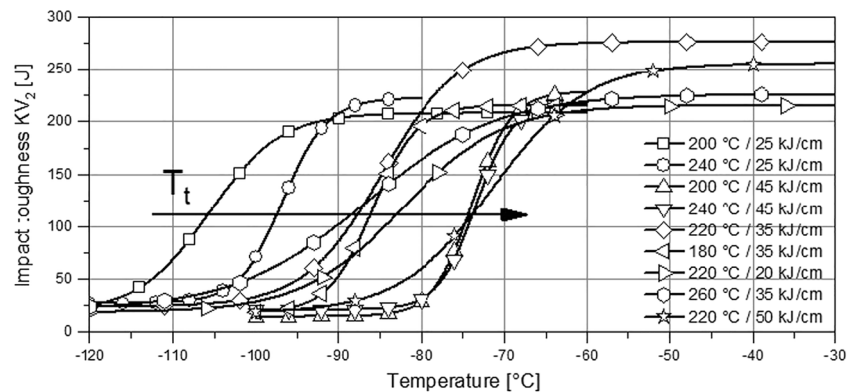
In the following, cracks are shown which were examined by optical light microscopy using weld cross sections. Figure 4 shows a macrograph (a) of a weld seam as well as detailed images of the cracks on the left (b) and right (c) sides. In this example, the heat input per unit length was 50 kJ/cm . The preheat/interpass temperature was 220°C . In addition to the primary cracks on the surface, which are starting from the

weld toe and run almost perpendicular to the direction of loading, there are numerous smaller side cracks parallel to the fusion line. The crack path, characteristic for SRC, runs along the PAGB within the CGHAZ and stops after approx. 3 mm in the fine-grained zone or in the base material. The surface of the primary cracks is oxidized, which is due to the high temperatures during the PWHT and the atmospheric contact.

The enlarged representation of a side crack in Fig. 4 (d) also reveals oxidized crack surfaces. In the coarse-grained, bainitic structure finely dispersed precipitates can be seen inside the grain. The clearly visible PAGB is an indication of the increased enrichment of certain alloying elements, carbides, and/or impurities or the formation of pores.

Figure 5 shows the SEM images of the crack site already acquired by light microscopy in Fig. 4 (b). On the polished unetched surface, the intergranular crack propagation can be seen, with oxidized crack surfaces. The SEM investigations reveal micropores which have formed along the PAGB. Micropores near the crack, especially in the area in front of the crack tip, are a further indication for SRC often documented in the literature [6, 32–35]. Figure 5 (d) (right) shows a further detailed view as well as the qualitative distribution of the alloying elements along the PAGB (e–h). Energy dispersive X-ray spectroscopy (EDX) revealed a significant accumulation of chromium and molybdenum, which is an indication for an increased grain boundary carbide precipitation.

Fig. 3 Influence of heat control on notched bar impact energy (KV_2 -T curve), notch location: heat-affected zone



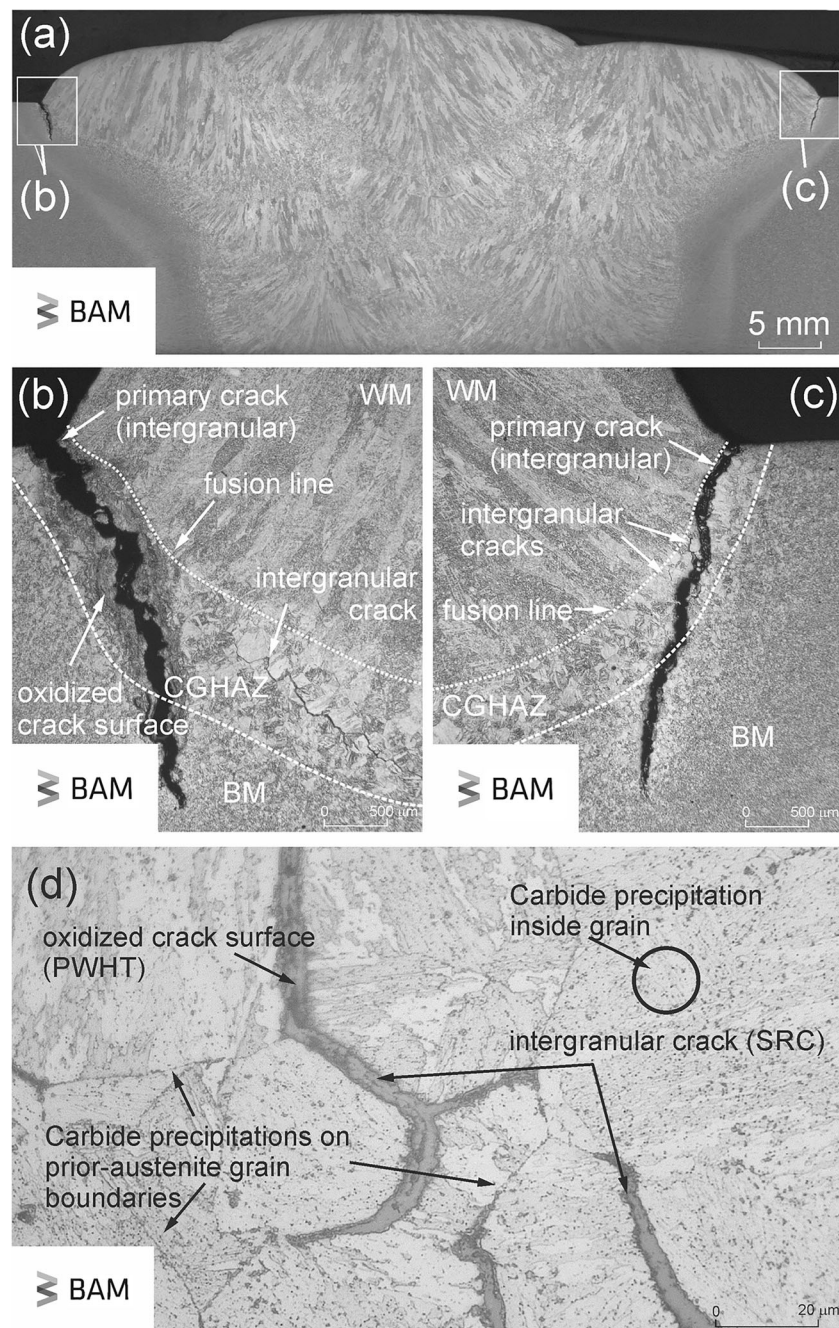


Fig. 4 Cross section of the weld seam (a) with cracks in the area of the right and left weld toe, detailed representation (b, c) of the cracks (primary crack and secondary crack) with intergranular crack path and oxidized crack surface of the primary crack, crack start in the CGHAZ, crack stop in the fine-grained zone or in the base material and detail of a SRC in the

HAZ (d), intergranular crack path with oxidized surface, carbide precipitates or pores on the PAGB, finely distributed carbide precipitates within the grains (welding heat input per unit length 50 kJ/cm, preheat/interpass temperature 220 °C)

Also, the measurement indicated carbon along the grain boundary. However, the determination of carbide concentration using EDX is not appropriate for low carbon contents as in case of this steel.

Transmission electron microscopic investigations were used to identify the precipitates along the cracks and the PAGB. Figure 6 (top) shows an overview of an SRC filled

with oxidation products along the PAGB within the HAZ. The oxidation products were identified in the marked area by energy-dispersive X-ray spectroscopy (EDX) as nanocrystalline magnetite Fe_3O_4 and chromium oxide Cr_2O_3 , as well as coarser magnetite. The EDX-analysis of the oxidized area shows a different precipitation behavior of the main alloy components along the oxidized crack flank.

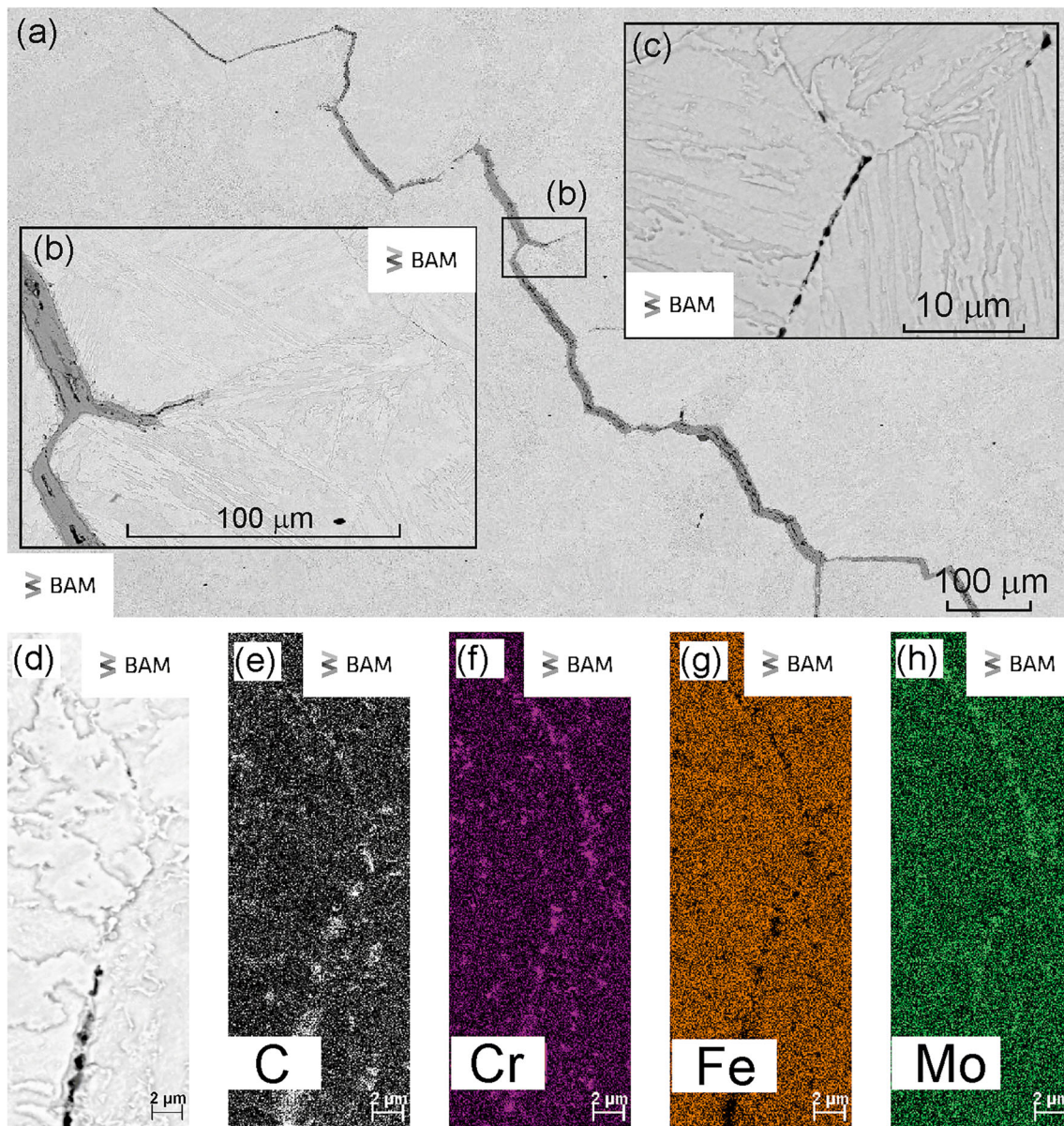


Fig. 5 SEM image of a SRC with intergranular crack path (a), detailed view of the crack area, with oxidized crack surface (b), detailed view of a PAGB with pores (c) and detail view (SEM) of a PAGB (d), qualitative

distribution of the alloying elements carbon (e), chromium (f), iron (g), and molybdenum (h), welding heat input per unit length 50 kJ/cm, preheat/interpass temperature 220 °C

Mo, Cr, and Mn are found along the interface between oxide layer and steel matrix. However, while Mo precipitates as a narrow band, Cr and Mn are heterogeneously distributed in islands. It can be assumed that the islands were formed by the oxidation of Cr and Mn-rich carbides, which were previously precipitated along the PAGB. In these areas enrichments of V can also be found. However, carbides cannot be detected due to the strong oxidation of the crack flank, so that additional investigations were carried out in the crack-free area of the HAZ without oxidation.

Figure 6 shows the brightfield image of a PAGB (a), the diffraction image from the SAED analysis (b) and the EDS

spectrum (c) of a carbide identified as M_6C . TEM investigations in the crack-free area also show enrichments of the alloying elements Mo, Cr, and V in the form of precipitates (carbides, M_6C) along the PAGB. According to [36–38], precipitates of this type are unusual for the steel under investigation and can only be expected after prolonged aging at higher temperatures. Assuming that the precipitation processes are accelerated by stresses or microplastic deformations as a result of the restraint, additional TEM analyses were performed on specimens welded without restraint. The results of the TEM analyses in the HAZ of the restrained and the unrestrained welded and heat-treated specimens are shown in Fig. 7.

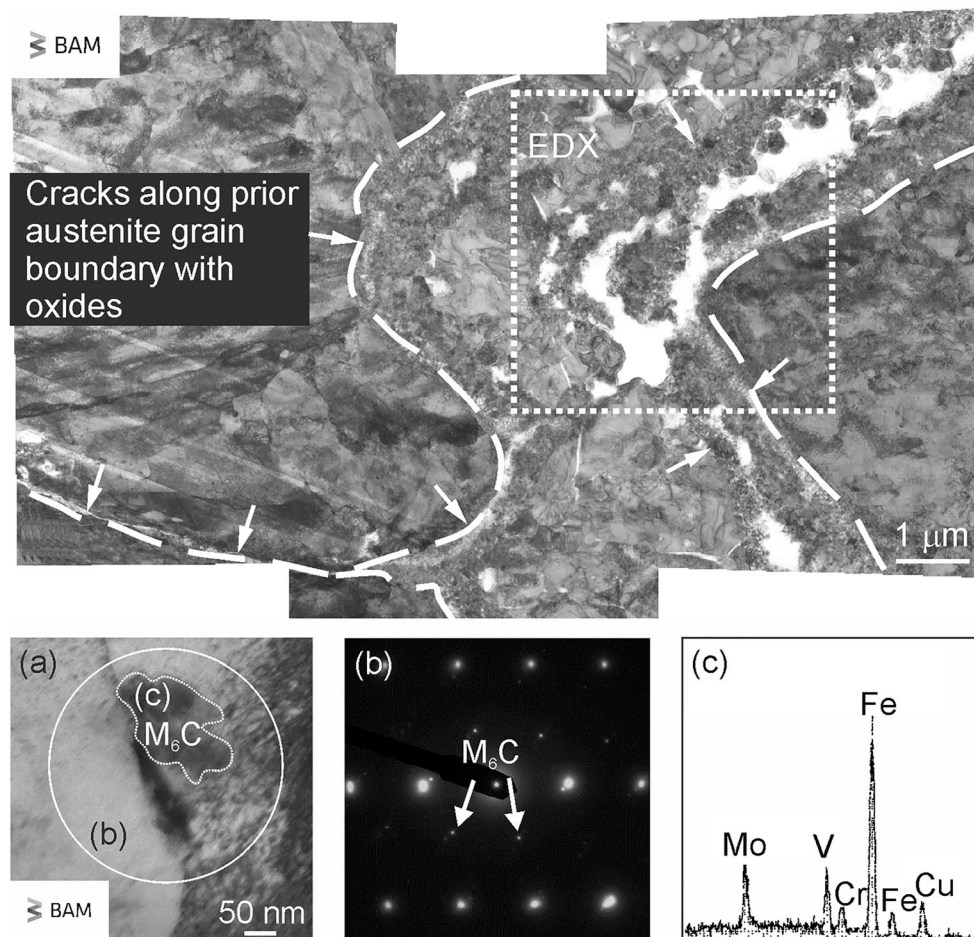


Fig. 6 Brightfield image of a scanning electron microscope (STEM-BF), SRC along the PAGB within the HAZ, filled with oxidation products (nanocrystalline (Fe, Cr)₃O₄ and coarser Fe₃O₄) (top), and Brightfield image (STEM-BF) of an M₆C carbide on a PAGB in the HAZ (a),

diffraction image from SAED analysis selected area electron diffraction, reflexes from (331)M₆C, (224)M₆C, and [−113] orientation of surrounding α-matrix (b), EDS spectrum of the M₆C carbide (c) (right), welding heat input per unit length 20 kJ/cm, preheat/interpass temperature 220 °C

In contrast to the restrained specimens, the unrestrained ones show neither cracks in the HAZ nor in the weld metal. Although, in both specimens there are numerous precipitates along the PAGB. However, while Cr, Mo, and V enrich in the carbides under restraint, mainly Cr is present in the carbides of the unrestrained specimens. Furthermore, the carbides in the unrestrained specimens were identified as M₂₃C₆, whereas M₆C was detected under restraint. M₂₃C₆ is formed during aging before M₆C [3, 36, 39–43]. As the TEM investigations were performed just for a single set of welding parameters, a critical stress level cannot be derived. Nevertheless, as M₆C was identified for the lowest heat input of this study, it is assumed that the mechanisms are similar for higher heat input associated with higher stress. From the impact toughness results (Fig. 3) which were observed on specimens without SRC, it is supposed that there is a general sensitization of the material due to the accelerated precipitation. This needs to be verified by

further analysis not only of the grain boundaries but also inside the grains.

In summary, it can be stated that the aging of the creep-resistant steel 13CrMoV9-10 is accelerated during PWHT under restraint. This leads to early and increased precipitation of carbides of type M₆C, which accumulates along the PAGB. In previous investigations, on small scale specimens, however, carbides of this type could only be detected after long annealing times. Thus, Výrostková et al. [36] and Kroupa et al. [41] detect M₆C only at V contents >0.12% and annealing times >100 h. Tamaki et al. [3, 44, 45] and Baker and Nutting [40] also observed the precipitation of M₂₃C₆ and M₇C₃, which only formed stable carbides of type M₆C after longer annealing times. In the present investigations, the increased grain boundary precipitation also correlates with a significant decrease in the notched bar impact energy of the specimens welded under restraint (see Fig. 3).

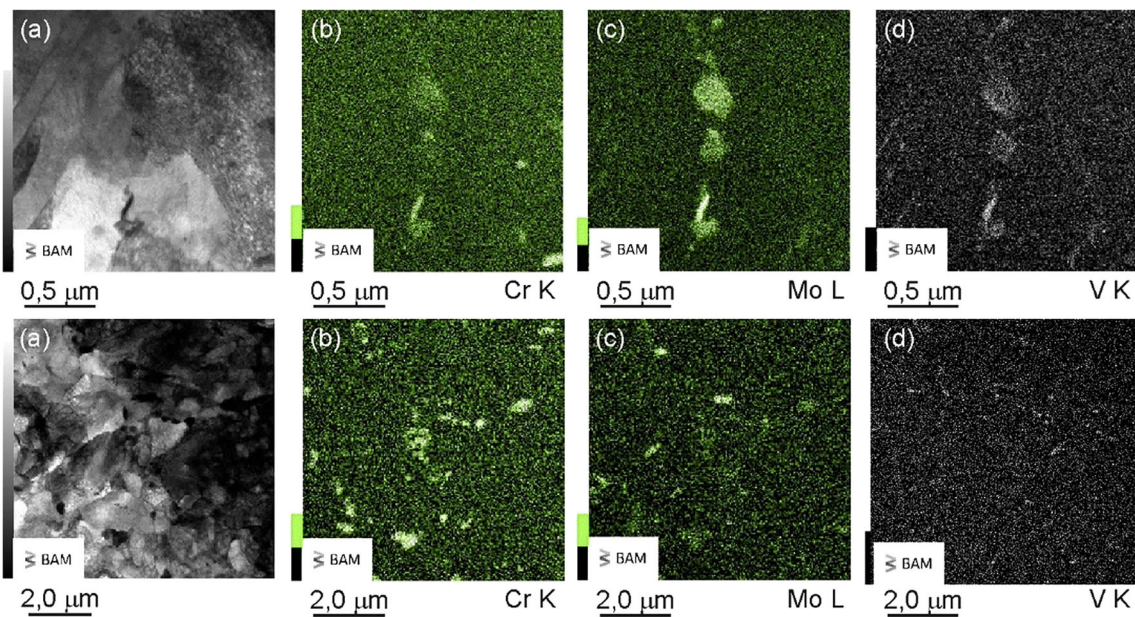


Fig. 7 Restrained specimen (top): brightfield image (STEM-BF) of a PAGB in the HAZ (a), distribution of the main alloying elements chromium (b), molybdenum (c), vanadium (d), EDX analysis and unrestrained specimen (bottom): brightfield imaging (STEM-BF) of PAGB

in the HAZ (a), distribution of the main alloying elements chromium (b), molybdenum (c), vanadium (d), EDX analysis (welding heat input per unit length 20 kJ/cm and preheat/interpass temperature 220 °C

4 Conclusions

1. The welding heat control has a significant effect on the SRC formation during PWHT under restraint. Cracking is influenced by the interaction of mechanical, thermal, and material factors. Cracks mainly occurred at the transition of the weld metal into the HAZ (weld toe), promoted by the stress rise due to the notch effect.
2. The consideration of the structural shrinkage restraint, both during the welding process and during the subsequent heat treatment, is necessary, as the resulting microstructure affects the mechanical properties of the welded joint. In the present tests, a pronounced dependence of the heat input on the notched bar impact energy of the HAZ could be determined, which leads to a shift of the transition temperature to higher temperatures with increasing heat input. This is also related to an accelerated carbide precipitation caused by welding under restraint.
3. The acoustic emission analysis during the PWHT enabled the observation of the SRC initiation in the temperature range between 300 and 500 °C. Hence, SRC occurred already during heating and minor during holding at maximum temperature when a slow heating rate of 60 K/h is applied.
4. Based on SEM and TEM analyses of the HAZ, it was demonstrated that the aging of the creep-resistant steel 13CrMoV9-10 is accelerated under restraint (i.e., under load). This leads to early and increased precipitation of carbides of type M_6C , which accumulate along the PAGB. In contrast, specimens welded without restraint

showed only carbides of type $M_{23}C_6$. Therefore, small-scale tests may not be suitable for characterizing thick-walled welded joints. The shown interaction of metallurgy and mechanical load requires tests which adequately reproduce the occurring stresses.

Funding Open Access funding enabled and organized by Projekt DEAL.

References

1. Boniszewski T (1971) Metallurgical aspects of reheat cracking of weldments in ferritic steels. In: heat-treatment aspects of metal-joining processes, Proceedings of the Biennial Conference organized by the Heat Treatment Joint Committee of the Iron and Steel Institute, the Institute of Metals and Institution of Metallurgist (London: 8–9 December), p. 29–41
2. Mayr P (2007) Evolution of microstructure and mechanical properties of the heat affected zone in B-containing 9% chromium steels. Diss. Graz: Graz University of Technology – Faculty of Mechanical Engineering – Institute for Materials Science, Welding and Forming
3. Tamaki K, Suzuki J, Nakaseko Y, Tajiri M (1984) Effect of carbides on reheat cracking sensitivity – (Study of Reheat Cracking of Cr-Mo Steels Report 3). *Trans Jpn Weld Soc* 15(1):8–16
4. Materials and Fabrications of 2 1/4 Cr-1Mo, 2 1/4 Cr-1Mo-1/4V, 3Cr-1Mo, and 3Cr-1Mo-1/4V Steel Heavy Wall Pressure Vessels for High-temperature, High-pressure Hydrogen Service, API Recommended Practice 934-A, second edition, May 2008, Addendum 1, February 2010, American Petroleum Institute
5. Briant CL, Benerji SK (1978) Intergranular failure in steel: the role of grain boundary composition. *Int Metals Rev* 4:164–199

6. Chauvy C, Pillot S (2009) Prevention of weld metal reheat cracking during Cr-Mo-V heavy reactors fabrication. 2009 ASME pressure vessels and piping division conference. ASME, Prague, Czech Republic, p. 1–9
7. Tamaki K, Suzuki J, Kawakami H (2004) Metallurgical factors affecting reheat cracking in HAZ of Cr-Mo steels. Proceedings of the Finnish-German-Japanese Joint International Seminar on Mechanical Approaches to New Joining Process, p. 155–168
8. Hunter ANR (1982) Reheat cracking in 2.25Cr1Mo submerged arc weld metal, Part 1 Materials, welding and testing. *Metal Construct* 14(4):198–201
9. Bruscato R (1970) Temper embrittlement and creep embrittlement of 2 1/4 Cr-1 Mo Shielded Metal-Arc weld deposits. *Weld J Res Supp* p. 148s–156s
10. Hunter ANR (1982) Reheat cracking in 2.25Cr1Mo submerged arc weld metal, Part 2 Results and discussion. *Metal Construct* 14(5): 266–270
11. Lalam SH, Bhadeshia HKDH, MacKay DJC (2000) Bruscato factor in temper embrittlement of welds. *Sci Technol Weld Join* 5(5):338–340
12. Dhooge A, Dolby RE, Sebillie J, Steinmetz R, Vinckier AG (1978) A review of work related to reheat cracking in nuclear reactor pressure vessel steels. *Int J Press Vessel Pip* 6:329–409
13. Bentley KP (1964) Precipitation during stress relief of welds in Cr-Mo-V steels. *Br Weld J* p. 507–515
14. Watanabe T, Warren FS (1983) A study of reheat cracking in weld heat-affected zone of high strength steel. *Trans Jpn Weld Soc* 14(2):37–44
15. Nakamura N, Wnjo T, Kikuchi Y (1992) Effects of heat-affected zone microstructure on reheat cracking susceptibility of Cr-Mo steels. *Weld Int* 6(6):436–442
16. Nawrocki J, DuPont J, Robino C, Marder A (2000) The stress-relief cracking susceptibility of a new ferritic steel – Part I: single-pass heat-affected zone simulations. *Weld J*:355s–362s
17. Swift RA, Rogers HC (1976) Study of creep embrittlement of 2,25 Cr-1Mo steel weld metal. *Weld World* 7:188s–199s
18. Watanabe J, Shindo Y, Murakami Y, Adachi T, Ajiki S (1974) Temper embrittlement of 2 1/4 Cr-1Mo pressure vessel steel. Proceedings of the ASME 29th Petroleum Mechanical Engineering Conference, Dallas, TX, USA
19. Chauvy C (2009) Reheat cracking of weld metal A542D. In: A program to upgrade materials and process standards for fabrication of heavy wall vessels of 2.25 Cr - 1Mo - 0.25V alloy for service with hydrogen at high pressure and temperatures. Materials Properties Council Inc
20. Chauvy C, Pillot S (2009) How to prevent reheat cracking of weld metal A542D. API meeting. API, Denver
21. Kotecki DJ (2014) Round robin of trace elements. *Weld World* 58(4):577–592
22. Kotecki DJ (2016) Fourth round robin report-trace elements in Cr-Mo-V steel weld metal. *Weld World* 60(4):639–643
23. Trent MC (2012) Development and use of a simple test method to evaluate reheat cracking sensitivity in the weld deposit region of a submerged arc weld. University of Tennessee, Knoxville
24. Tamaki K, Suzuki J (1983) Reheat cracking test on high strength steels by a modified implant test – (Study of reheat cracking of Cr-Mo steels, Report I). *Trans Jpn Weld Soc* Bd 14(2):33–38
25. DIN EN 10028-2 (2017) Flat products made of steels for pressure purposes - Part 2: Non-alloy and alloy steels with specified elevated temperature properties; German version EN 10028-2:2017.
26. American Welding Society (1996) Recommended practices for welding of chromium-molybdenum steel piping and tubing: ANSI/AWS D10.8-96, an American National Standard. American Welding Society p. 12
27. Berzolla A, Bertoni A, Bocquet P, Hauck G (2008) The New 2.25Cr and 3Cr-1Mo- 0.25V steels for pressure vessels operating in hydrogen environment. A Joint European Research Contract. IIW Doc XI-897-08, p. 577–606
28. Lausch T (2015) Zum Einfluss der Wärmeführung auf die Rissbildung beim Spannungsarmglühen dickwandiger Bauteile aus 13CrMoV9–10. Dissertation, BAM Bundesanstalt für Materialforschung und -prüfung, BAM Dissertationsreihe Band 134. Berlin: Otto-von-Guericke-Universität Magdeburg (in German)
29. Kromm A, Lausch T, Schroepfer D, Rhode M, Kannengiesser T. Influence of welding stresses on stress relief cracking during heat treatment of a creep-resistant 13CrMoV steel, Part I: Effect of heat control on welding stresses and stress relief cracking. IIW-Doc. II-2117-19. <https://doi.org/10.1007/s40194-020-00875-6>
30. Kromm A, Lausch T, Schroepfer D, Dixneit J, Hannemann A, Kannengiesser T (2018) From the field to the lab: real scale assessment of stresses in welded components. *Mater Perform Characterizat* 7(4):574–593. <https://doi.org/10.1520/MPC20170103>
31. Lausch T, Kannengiesser T, Schmitz-Niederer M (2013) Multi-axial load analysis of thick-walled component welds made of 13CrMoV9-10. *J Mater Process Technol* 213(7):1234–1240
32. Meitzner CF (1975) Stress relief cracking in steel weldments. *Weld Res Counc Bull* 211:1–17
33. Kussmaul K, Blind D, Ewald J (1977) Investigation methods for the detection and study of stress-relief cracking. *Int J Press Vessel Pip* 5:159–180
34. Nawrocki JG, DuPont JN, Robino CV, Marder AR (2001) The stress-relief cracking susceptibility of a new ferritic steel – Part 2: multi-Pass heat-affected zone simulations. *Weld J Res Suppl* p. 18s–24s
35. Nawrocki JG, DuPont JN, Robino CV, Puskar JD, Marder AR (2003) The mechanisms of stress-relief cracking in a ferritic alloy steel. *B Weld J* p.25s–35s
36. Výrostková A, Kroupa A, Janovec J, Svoboda M (1998) Carbide reactions and phase equilibria in low alloy Cr–Mo–V steels tempered at 773–993 K. Part I: experimental measurements. *Acta Mater* 46(1):31–38. [https://doi.org/10.1016/S1359-6454\(97\)00238-3](https://doi.org/10.1016/S1359-6454(97)00238-3)
37. Tao P, Zhang C, Yang Z-G, Takeda H (2010) Evolution and coarsening of carbides in 2. 25Cr-1Mo steel weld metal during high temperature tempering. *J Iron Steel Res Int* 17(5):74–78. [https://doi.org/10.1016/S1006-706X\(10\)60103-3](https://doi.org/10.1016/S1006-706X(10)60103-3)
38. Working Group Electron Microscopy of Materials Committee Steel Institute VDEh (2003) Atlas of precipitates in steels. Verlag Stahleisen GmbH, Düsseldorf ISBN: 3–514- 00681-4
39. Lundin CD and Khan KK (1996) Fundamental studies of the metallurgical causes and migration of reheat cracking in 1 1/4Cr-1/2Mo and 2 1/4Cr-1Mo Steels. Welding Research Council Bulletin, p. 409
40. Baker RG and Nutting J (1959) The tempering of 2 1/4%Cr-1%Mo steel after quenching and normalizing. *Journal of the Iron and Steel Institute*, p. 257–268
41. Kroupa A, Výrostková A, Svoboda M, Janovec J (1998) Carbide reactions and phase equilibria in low-alloy Cr–Mo–V steels tempered at 773–993 K. Part II: theoretical calculations. *Acta Materialia*, Bd 46(1): 39–49. [https://doi.org/10.1016/S1359-6454\(97\)00239-5](https://doi.org/10.1016/S1359-6454(97)00239-5)
42. Janovec J, Svoboda M, Výrostková A, Kroupa A (2005) Time-temperature-precipitation diagrams of carbide evolution in low alloy steels. *Mater Sci Eng A Bd* 402(1–2):288–293. <https://doi.org/10.1016/j.msea.2005.04.048>
43. Tamaki K, Suzuki J, Li M-L (1993) Influence of vanadium carbide on reheat cracking of Cr-Mo steels – (Study of Reheat Cracking of Cr-Mo Steels Report 10). *Trans Jpn Weld Soc* 24(2):87–93
44. Tamaki K, Suzuki J (1982) Precipitation of carbides during tempering of Cr-Mo steels. Research reports of the Faculty of Engineering, Mie University, 7, p. 39–52
45. Kawakami H, Tamaki K, Suzuki J, Takahashi K, Imae Y, Ogusu S (2011) Effect of coarse carbide particle on SR embrittlement in HAZ of 2.25Cr-1Mo steel. *Weld World* 55:78–85